

Spin splitting tunable optical band gap in polycrystalline GdN thin films for spin filteringG. L. S. Vilela^{1,2,*}, G. M. Stephen^{3,4}, X. Gratens⁵, G. D. Galgano^{5,6}, Y. Hou¹, Y. Takamura⁷,
D. Heiman^{1,3,†}, A. B. Henriques⁵, G. Berera⁸ and J. S. Moodera^{1,9,‡}¹*Plasma Science and Fusion Center and Francis Bitter Magnet Laboratory, Massachusetts Institute of Technology, Cambridge, Massachusetts 02139, USA*²*Física de Materiais, Escola Politécnica de Pernambuco, UPE, Recife PE 50720-001, Brazil*³*Department of Physics, Northeastern University, Boston, Massachusetts 02115, USA*⁴*Laboratory for Physical Sciences, College Park, Maryland 20740, USA*⁵*Laboratório de Magneto-Óptica, Instituto de Física, Universidade de São Paulo, São Paulo, SP 05508-090, Brazil*⁶*Departamento de Física, Universidade Federal de Ouro Preto, Ouro Preto, Minas Gerais 35402-136, Brazil*⁷*School of Engineering, Tokyo Institute of Technology, 2-12-1 Ookayama, Meguro-ku, Tokyo 152-8550, Japan*⁸*Department of Materials Science and Engineering, Massachusetts Institute of Technology, Cambridge, Massachusetts 02139, USA*⁹*Department of Physics, Massachusetts Institute of Technology, Cambridge, Massachusetts 02139, USA*

(Received 4 June 2023; revised 10 January 2024; accepted 12 January 2024; published 2 February 2024)

Rare-earth nitrides, such as gadolinium nitride (GdN), have great potential for spintronic devices due to their unique magnetic and electronic properties. GdN has a large magnetic moment, low coercivity, and strong spin polarization suitable for spin transistors, magnetic memories, and spin-based quantum computing devices. Its large spin splitting of the optical band-gap functions as a spin filter that offers the means for spin-polarized current injection into metals, superconductors, topological insulators, two-dimensional layers, and other novel materials. As spintronics devices require thin films, a successful implementation of GdN demands a detailed investigation of the optical and magnetic properties in very thin films. With this objective, we investigate the dependence of the direct and indirect optical band gaps (E_g) of half-metallic GdN, using the trilayer structure AlN (10 nm)/GdN (t)/AlN (10 nm) for GdN film thickness t ranging from 6 to 350 nm, in both paramagnetic (PM) and ferromagnetic (FM) phases. Our results show a band gap of 1.6 eV in the PM state, while in the FM state the band gap splits for the majority (0.8 eV) and minority (1.2 eV) spin states. As the GdN film becomes thinner, the spin-split magnitude increases by 60%, going from 0.290 to 0.460 eV. Our results point to methods for engineering GdN films for spintronic devices.

DOI: [10.1103/PhysRevB.109.L060401](https://doi.org/10.1103/PhysRevB.109.L060401)

Introduction. Spintronic devices based on rare-earth nitrides (RENs) are of great interest since they present both semiconducting and ferromagnetic properties, making these materials suitable for exploiting the spin of carriers in fundamental and applied research [1,2]. Among many RENs, gadolinium nitride (GdN) is especially promising for implementations that aim to explore the electron's spin to store, process, and transmit information. The advantageous properties of GdN are its high degree of spin polarization, half-metallic behavior that is useful for spin filtering, sizable ferromagnetic transition temperature of ~ 70 K, and large magnetic moment of $7 \mu_B/\text{Gd}^{3+}$ due to fully occupied $4f$ electronic states [3–8]. The use of this material in selective transmission of electrons based on their spin orientation finds applications in magnetic tunnel junction, spin valves, spin transistors, and spin-based quantum computing, where the electron's spin state encodes and processes quantum infor-

mation. In this context, the spin-filtering ability promotes an efficient way to inject and manipulate the spin current [9–14].

Due to its high oxophilicity, GdN easily reacts in air forming Gd_2O_3 , which can cause significant changes in its electronic and magnetic properties [15,16]. The growth of stoichiometric GdN thin films, with low levels of oxygen, is very challenging and requires rigorous control of the synthesis. This challenge has led to some disagreement in the literature regarding the electronic properties of GdN films, but most results point to its semiconducting behavior with an average band gap of 1.2–3 eV at room temperature [5,17,18]. In addition to controlling the stoichiometry, to combine GdN with novel materials that are aimed at investigating interface and spin phenomena, it is crucial to obtain atomically flat surfaces with a high degree of crystallinity, large magneto-optical effects, thermal stability, and tunable band-gap energy. These properties depend on the film's strain, thickness, nitrogen vacancies, amount of oxygen impurities, parameters that depend on growth and postgrowth processes, as well as protective layer and substrate choices.

In this work, we investigate the optical and magnetic properties of a set of polycrystalline GdN thin films with thickness ranging from $t = 6$ –350 nm. The AlN (10 nm)/GdN (t)/AlN

*gilvania.vilela@upe.br

†Heiman@neu.edu

‡Moodera@mit.edu

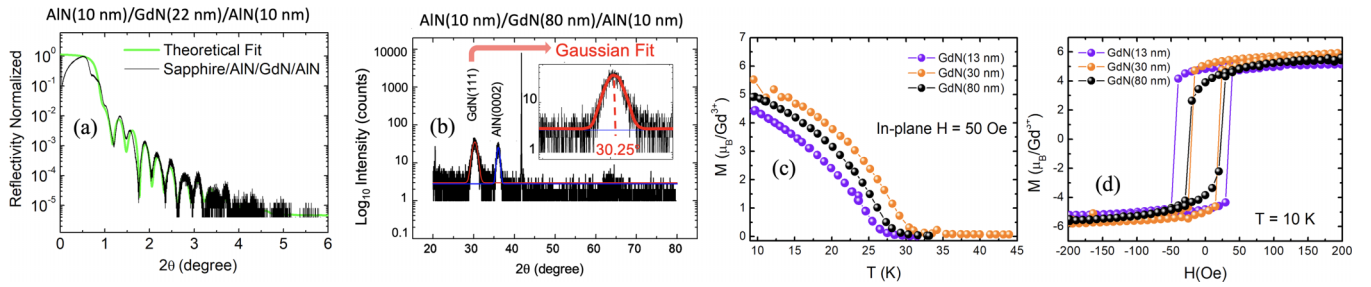


FIG. 1. (a) X-ray reflectivity for the rf-sputtered AlN (10 nm)/GdN (22 nm)/AlN (10 nm) and theoretical fit used to obtain the GdN film thickness. (b) High-resolution x-ray diffraction pattern for AlN (10 nm)/GdN (350 nm)/AlN (10 nm) on a (0001)-oriented sapphire (Al_2O_3) substrate. (c) In-plane field cooled magnetization at 50 Oe for GdN thicknesses of 13, 30, and 80 nm. (d) Magnetization (M) vs in-plane applied magnetic field (H) at $T = 10$ K for AlN (10 nm)/GdN (t)/AlN (10 nm) structures, with $t = 13, 30,$ and 80 nm.

(10 nm) structures were reactively sputtered on sapphire (0001) substrates in a UHV sputtering system, grown at 700°C in a pressure of 2.8 mTorr (mixture of 40% N_2 and 60% Ar). Measurements using a superconducting quantum interference device (SQUID) magnetometer confirm that the GdN films are magnetic with magnetization saturation of $6 \mu_B/\text{Gd}^{3+}$ and a Curie temperature of ~ 30 K, in agreement with previous reports, and x-ray diffraction data confirms a polycrystallinity [5, 18, 19]. Direct and indirect band-gap energies as a function of the films' thicknesses are determined from analysis of the squared-absorption spectra (α^2) and $\sqrt{\alpha}$ using extrapolated curves, respectively. The band-gap energy in the paramagnetic (PM) phase, at 300 K, reveals a direct band gap of ~ 1.6 eV with no dependencies on the spin, whereas this value decreases and splits to 1.2 and 0.8 eV, approximately, in the ferromagnetic (FM) phase at 6 K. In the low-temperature FM state a well-separated spin-split band energy of $\Delta E = E_\uparrow - E_\downarrow \approx 0.4$ eV is found, which confirms a giant optical spin splitting in the GdN films, where E_\uparrow and E_\downarrow correspond to the band gaps of the majority and minority states. We also observe that the splitting magnitude depends strongly on the GdN film thickness, going from 0.290 eV for a 350-nm-thick film to 0.460 eV for a 6-nm-thick film—an increase of about 60%.

Since the investigated GdN films are polycrystalline, the extensively used Tauc method suitable for determining the band gap of amorphous semiconductors was not applied in our analysis [20]. Zanatta proposed the use of sigmoid (Boltzmann) functions for more accuracy, and showed that for crystalline Si, Ge, and GaAs the α^2 extrapolated curve is in good agreement with the Boltzmann analysis [21]. For simplicity, we used α^2 for direct band-gap estimation.

Sample preparation, crystal structure, and magnetic properties. GdN thin films with thickness ranging from 6.3 to 350 nm were deposited on (0001)-oriented sapphire substrates, with buffer and capping layers of 10-nm-thick aluminum nitride (AlN) films to avoid oxidation. The growth process of AlN and GdN took place in a high vacuum sputtering chamber with a base pressure below 5×10^{-8} Torr. To improve the substrate's surface crystallinity and film quality, prior to deposition the sapphire substrates were annealed in a quartz-tube oven at 1100°C for 8 h in an O_2 atmosphere. After the annealing treatment, the substrates were cleaned in an ultrasonic tank first in acetone, and then in isopropanol before transferring into the load lock chamber and subsequently to

the main sputtering chamber. Inside the growth chamber the substrates were slowly heated up to 700°C for degassing followed by the deposition process. Targets of 99.99% purity of Al and Gd were presputtered for 10–20 min in a controlled atmosphere composed of 60% argon and 40% N_2 before reactively growing AlN and GdN on the substrates. The AlN deposition rate was approximately 1.0 nm/min, at 700°C , with rf power of 150 W and a working pressure of 1.2 mTorr. The GdN films deposition rate was approximately 2 nm/min, deposited at 700°C , in a working pressure of 2.8 mTorr and a DC power of 50 W. The deposition rates and film's thickness were estimated using x-ray reflectometry as shown in Fig. 1(a). The high-resolution x-ray diffraction patterns for GdN (80 nm) shown in Fig. 1(b) confirm a preferentially orientated growth along the (111) direction in agreement with previous investigations [22, 23].

Besides having good crystallinity, it is important that GdN films have a large magnetic moment as confirmed by SQUID measurements, shown in Figs. 1(c) and 1(d). The field-cooled magnetization curves of GdN film in the trilayer AlN (10 nm)/GdN (t)/AlN (10 nm) show a magnetization saturation varying from $4.5 \mu_B/\text{Gd}^{3+}$ to $5.5 \mu_B/\text{Gd}^{3+}$ for an in-plane $H = 200$ Oe, as the GdN's thickness ranges from $t = 13$ to 80 nm. The FM critical temperature (T_C), was near 30 K, measured with an applied in-plane magnetic field of 50 Oe, as shown in Fig. 1(d), which agrees with previous reports [5, 18, 19]. The coercivity (H_c) is larger (40 Oe) for the thinner 13-nm-thick GdN film and decreases to ~ 20 Oe for $t = 30$ and 80 nm.

The observed magnetic moments are smaller than the theoretical expected value of $7 \mu_B/\text{Gd}^{3+}$. One of the reasons is the applied magnetic field of 200 Oe is not enough to saturate the film; instead it is necessary $\sim 10^4$ Oe [11, 24, 25]. Other facts might affect the magnetic moment in GdN films: (i) nitrogen vacancies cause changes in the lattice constant, magnetization, and conductivity, since N acts as a dopant; (ii) oxygen contamination that also acts as a dopant; and (iii) lattice parameter strains caused by a mismatch between the substrate and film [1, 7, 22, 26]. Khazen *et al.* showed how an extension of 2.4% in the lattice parameter of GdN films, compared to the bulk value of 4.99 Å, which promotes substantial changes in the magnetization behavior and reduces the magnetic moment [25]. As shown in the inset of Fig. 1(b), the GdN(111) peak for the 80-nm-thick film is located at $2\theta = 30.25^\circ$ determined by a Gaussian fit. This corresponds to a lattice parameter of

5.11 Å—an extension of 2.4%. The same analysis for the 350-nm-thick GdN presented a (111) peak located at $2\theta = 30.51^\circ$ with a lattice parameter of 5.07 Å, which corresponds to an extension of 1.6%. The full width at half maximum (FWHM) of the XRD (111) peak for GdN (80 nm) was 1.42° and the crystallite size estimation was 5.8 nm. For GdN (350 nm) these values became 1.01° and 7.8 nm, respectively. The FWHM increase indicates a relaxation of the tensile stress and a reduction in the number of grains due to their coalescence leading to a more crystalline film as GdN becomes thicker.

Finally, the twinned domains present in GdN grains, influenced by the hexagonal surface symmetry of the AlN template/buffer layer, could potentially impact the magnetic and optical properties. This is attributed to the alterations in structural and surface properties observed in group-III rare-earth nitrides [27,28].

Optical band-gap properties. Engineering the optical band gap in GdN thin films by controlling its magnetic state and thickness leads the way for its implementation in spintronic devices. The temperature dependence of the semiconductor's band gap can be different in bulk and thin-film morphologies due to factors such as quantum confinement and lattice strain effects. In bulk samples, the band gap typically increases as the temperature decreases partly due to the renormalization of electron-phonon interactions and partly due to lattice thermal expansions. As the temperature decreases, the phonon population also decreases leading to an increase of the band-gap energy, making it more difficult for electrons to be excited to the conduction band [29]. In most bulk semiconductors, the thermal expansion term is negligible in first approximation compared to the electron-phonon interaction [30]. In contrast, the band gap's temperature dependence in thin films is more complex. It is known that light absorption by electrons in semiconductors with restricted geometry like thin films, nanowires, and quantum dots are strongly dependent on the size [30–32]. This quantum confinement effect also gives rise to changes in the transition probabilities, which is a consequence of the electron's wave properties. Materials with dimensions on the order of the de Broglie wavelength show relevant quantum-mechanical effects with size-dependent optical properties. Models predict a decrease in phonon frequency and dielectric constant of semiconducting nanostructures leading to an increase of the band-gap energy as the material's size reduces, as confirmed by reported studies [33–35].

On the other hand, the lattice constant plays an important role in the optical, electronic, and magnetic properties of GdN thin films leading to changes on its spin-dependent band structure. Previous investigations showed how changes in the unit cell volume of GdN leads to half-metallic to semiconducting transformation [6]. At low temperatures, the lattice constant of the material shrinks, resulting in an increased interatomic bond strength, higher phonon frequencies, and reduced lattice vibrational amplitudes [36]. Also, the mismatch promotes extra strain in the interfaces, and thus affects the band gap. In sapphire/AlN/GdN/AlN, the differences among the thermal expansion coefficients of each material create a complex strain on GdN. The GdN lattice expansion coefficient is $8.7 \times 10^{-6}/\text{K}$, while for AlN this value is $4.2 \times 10^{-6}/\text{K}$, and for sapphire substrate it is $8.1 \times 10^{-6}/\text{K}$ [37–39]. As the

temperature decreases to 6 K, GdN's lattice parameter shrinks more than AlN's, in such a way that the lattice mismatch between GdN and AlN causes a tensile strain on GdN's surfaces, and a compressive strain on AlN's surface, which would lead to an increase in the band gap of GdN.

To better understand the role of thickness and temperature in a thin GdN layer, we measured the optical density (OD) spectra as a function of the photon energy ($E = h\nu$), at temperatures of 300 and 6 K, for AlN (10 nm)/GdN (t)/AlN (10 nm) trilayers on (0001) sapphire with $t = 6.3, 13, 22, 30, 80,$ and 350 nm [see Figs. 2(b) and 2(c)]. The absorption coefficient (α) was determined using the Beer-Lambert law that relates the amount of light absorbed by a material to its concentration, path length, and molar absorption coefficient. For a material with a uniform thickness, the relationship can be simplified as

$$\alpha = \frac{\text{OD}}{t}, \quad (1)$$

where t is the film's thickness. α^2 versus E plots were used to estimate the direct band-gap (E_g) energies of the GdN thin films via extrapolation of the linear portion of the curve to $\alpha^2 = 0$, as shown in Fig. 2(d), where $E_g = 1.6$ eV. The energy at which the extrapolated line intersects the energy axis corresponds to the direct band-gap energy E_g [40,41]. To determine the indirect band gap, the procedure is similar, but the analysis relies on extrapolating $\alpha^{1/2}$ versus E . The range of the photon energy in this investigation is well below that for the AlN band gap of ~ 6.1 eV and the sapphire band gap of ~ 9 eV [42–44]. Thus, the observed absorption spectra are clearly attributable to the GdN films. Figures 2(e) and 2(f) show α^2 vs $h\nu$ for $T = 300$ K, and $\alpha^{1/2}$ vs $h\nu$ for $T = 6$ K, respectively. To reduce errors in the band-gap determination due to drawing lines manually, we identified the linear portions of each curve (α^2 versus E) and fit the experimental data to $y = A + Bx$. The band gap was determined when $y = \alpha^2 = 0$, so $E_g = -A/B$. The uncertainty associated with this band gap was determined using

$$\sigma_{E_g} = \sqrt{\left(\frac{-1}{B}\sigma_A\right)^2 + \left(\frac{-A}{B^2}\sigma_B\right)^2}, \quad (2)$$

where σ_A and σ_B are the relevant uncertainties. Table I shows fitted values of the intercept (A) and slope (B) and their respective uncertainties that were used for determining the direct band gap at 300 K. The red data points in Fig. 3(d) show $E_g(t)$, where the solid curve is a guide for the eyes and the error bars are smaller than the data points. The direct band gap of the GdN films in the paramagnetic phase is around $E_{300\text{ K}} = 1.6$ eV and spans a region of GdN thickness ($13\text{ nm} < t < 80\text{ nm}$) where the gap increases as the thickness decreases, being attributed to quantum confinement. When samples are cooled down to 6 K they become FM, where the absorption spectra present more than one narrow linear deviation, indicating a spin-split band gap. Thus, in the magnetic state, the average minority (spin-down) band-gap energy is $E_\downarrow \approx 1.2$ eV, and the average majority (spin-up) band-gap energy is $E_\uparrow \approx 0.8$ eV, as shown by the blue data in Fig. 3(d), where the black dotted lines correspond to their average energy values. As the temperature decreases from 300

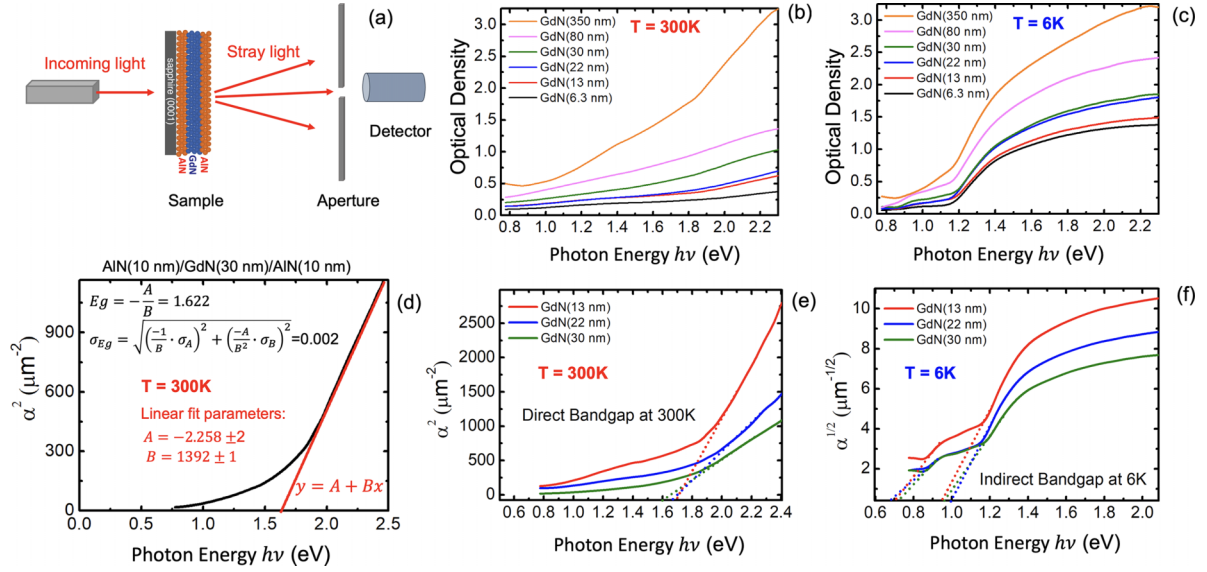


FIG. 2. (a) Illustration of the optical density acquisition apparatus composed of light source, sample, aperture, and light detector. (b) and (c) show the optical density spectra for the set of samples at 300 and 6 K. (d) shows how the direct optical band gap, at room temperature, for a $t = 30$ -nm-thick film was extracted from the squared-absorption coefficient (α) vs photon energy. The linear red fitted curve ($y = Ax + B$) is used to determine the band gap. (e) and (f) show α^2 and $\alpha^{1/2}$ vs the photon energy $E = h\nu$ for determining the direct and indirect optical band gaps of the GdN thin films, respectively. The dashed lines indicate the linear extrapolation to $y = 0$ where the intersection corresponds to the direct/indirect band-gap energy.

to 6 K, the band-gap variations are $E_{300\text{ K}} - E_{\downarrow} \approx 0.4$ eV for the minority state and $E_{300\text{ K}} - E_{\uparrow} \approx 0.8$ eV for the majority state. This observed band-gap reduction as the temperature decreases to 6 K suggests the shrinking of the lattice parameter in the volume of GdN overcomes the tensile strain effect at the interface of AlN/GdN that would lead to an increase in the band gap.

Finally, Fig. 3(a) is a very simplified illustration of the band structure of a semiconducting magnetic material in its paramagnetic and ferromagnetic phases. A more accurate calculation of the GdN band structure using local density approximation can be found in [17] for the paramagnetic and ferromagnetic states. The band gap in the PM phase is the same for electrons with spin up or spin down, whereas in the FM phase it depends on the spin orientation, and it splits into E_{\downarrow} and E_{\uparrow} . Figures 3(b) and 3(c) demonstrate α^2 vs $h\nu$ plots for the direct band gap of a 30-nm-thick GdN film in both paramagnetic (300 K) and ferromagnetic (6 K)

TABLE I. Intercept (A) and linear fit slope (B) and their respective uncertainties (σ_A and σ_B) from α^2 vs E plots for the AlN/GdN (t)/AlN structures as a function of GdN thickness (t). The direct band gap (E_g) and its uncertainty (σ_{E_g}) for GdN films at 300 K in eV units.

GdN film thickness (nm)	A	σ_A	B	σ_B	E_g	σ_{E_g}
6.3	-7320	30	4650	20	1.576	0.009
13	-7060	20	4069	7	1.736	0.005
22	-3620	20	2117	7	1.709	0.009
30	-2258	2	1392	1	1.622	0.002
80	-388.8	0.8	261.0	0.4	1.490	0.004
350	-229.2	0.9	137.6	0.4	1.665	0.008

phases, respectively. In the FM state, we observe a linear portion that extrapolates to $E_{\downarrow} = 1.192 \pm 0.006$ eV, and by zooming around 0.9 eV, as shown in the inset, we observe two linear portions that extrapolate to the energies of $E_{\uparrow 2} = 0.844 \pm 0.005$ eV and $E_{\uparrow 1} = 0.900 \pm 0.008$, with an average value of $E_{\uparrow} = 0.87 \pm 0.01$. This band-gap splitting appears for all GdN thicknesses investigated here, and a complete analysis is shown in Fig. 3(d). The filled blue points correspond to the minority band gap (E_{\downarrow}) and the unfilled blue points correspond to the majority band gap (E_{\uparrow}). The details are shown in the zoomed Figs. 3(e) and 3(f), respectively. These results show a giant optical spin splitting of the direct band gap at 6 K of $E_{\uparrow} - E_{\downarrow} \approx 0.4$ eV. The dependence of the direct band-gap spin splitting magnitude on the GdN film thickness is shown in Fig. 3(j). The black star and black circle points show the splitting with respect to $E_{\uparrow 1}$ and $E_{\uparrow 2}$, and the solid lines are guides for the eyes. As the thickness decreases, the spin splitting magnitude increases most likely due to two combined factors: (i) the strengthening of the quantum confinement as the GdN film becomes thinner and (ii) the reduction of the GdN's volume making the surface tensile strain on GdN more relevant, thus leading to a band-gap increase.

Figure 3(g) shows the same analysis for the indirect optical band gaps in the PM (red points) and FM states (blue filled and unfilled points). At room temperature (300 K) the indirect transitions occur at very small energies, whereas in the FM phase, we still observe two absorption lines with separation of ~ 0.4 eV that increases as film's thickness decreases reaching values of ~ 0.6 eV for the 6.3-nm-thick layer. The zoomed details are shown in Figs. 3(f) and 3(h).

Our experimental results show a good agreement with the (LSDA + U)-computed band structure for $U_d = 8.0$ eV reported by Trodahl *et al.* [17]. For a 200-nm-thick GdN film

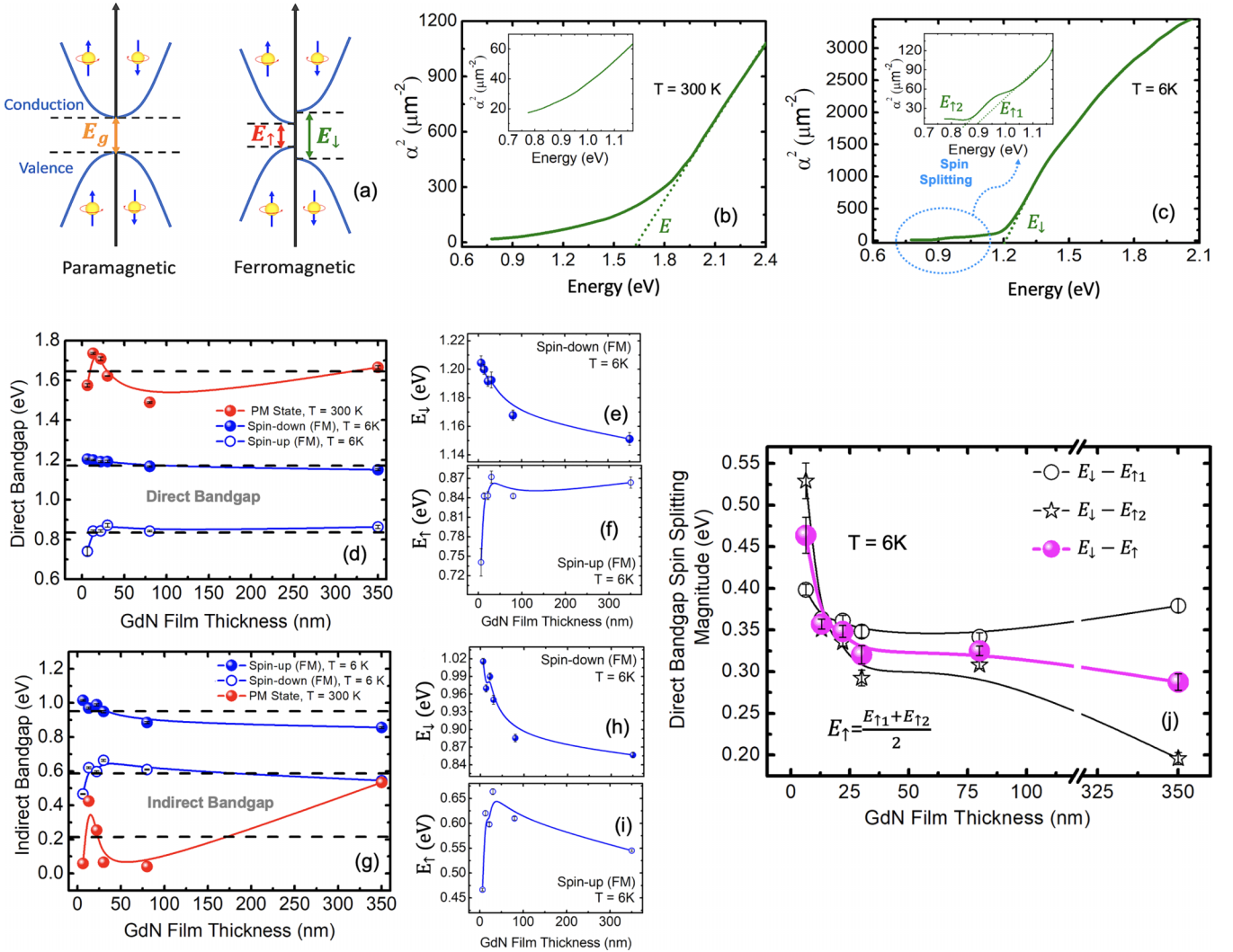


FIG. 3. (a) Illustration of the band structure of a magnetic semiconductor in the paramagnetic (left) and ferromagnetic (right) phases. In the PM phase, the band gap does not depend on the spin's orientation. (b) and (c) compare the α^2 vs E plots for obtaining the direct optical band gap of sapphire/AlN (10 nm)/GdN (30 nm)/AlN (10 nm) in the PM ($T = 300$ K) and FM ($T = 6$ K) phases. In the FM phase, shown in the inset of (c), we observe more than one linear portion that is related to the spin-split band gap. (d) and (g) show the direct and indirect optical band gaps dependence with the GdN film thickness at 300 and 6 K, where the black dotted lines correspond to their average energy values, and (e), (f), (h), and (i) are the zoomed direct and indirect band gaps for the minority and majority-spin states at 6 K. The spin splitting of the band gap is also present in the indirect transitions. (j) Dependence of the magnitude of the spin splitting as a function of the GdN thickness, showing that the splitting becomes larger as the film thickness decreases.

capped with 200 nm of GaN, they calculated a majority-spin gap of 0.91 eV in the ferromagnetic state at 6 K, and an average gap of 1.30 eV in the paramagnetic phase at 300 K, which represents a shift of 0.4 eV. The calculations also indicated an indirect-gap semiconductor with the direct gap at X and an indirect (Γ - X) gap of 0.43 eV (0.98 eV) in the ferromagnetic (paramagnetic) state. Our data showed an average majority-spin gap of around 0.84 eV at 6 K, and a gap of 1.6 eV at 300 K. For the indirect gap we estimated averages of 0.6 and 0.96 eV in the ferromagnetic phase and 0.2 eV in the paramagnetic phase.

Conclusions. We investigated a set of polycrystalline GdN thin films aiming to control its band gap and move towards their application as a spin-polarized source in spintronic devices such as spin transistors, tunneling magnetoresistance

(TMR) magnetic tunnel junctions, and spin valves. By varying the thickness from 6 to 350 nm we observed a room temperature direct band-gap average value of 1.6 eV with a variation of 0.24 eV as the thickness decreases. Upon cooling the films down to 6 K, in their ferromagnetic phase the direct band gap splits into two gaps of 1.2 and 0.8 eV, corresponding to the minority and majority-spin bands. This giant optical spin splitting of 0.4 eV confirms this material is suitable for spin-filtering applications. The same behavior appears in the indirect band gap with a splitting magnitude of 0.3 eV. The observed spin splitting magnitude ($E_{\uparrow} - E_{\downarrow}$) increased 60% as the GdN thickness decreased from 350 to 6 nm. This result sheds light on the manipulation and control of the optical and magnetic properties of the semiconducting GdN films with the potential for high spin polarization through the spin

splitting of the band gap. Further investigations should focus on determining the band-gap dependence on a larger range of temperature covering the details on the PM-FM transition, and performing x-ray measurements as a function of temperature to understand the role of thermal expansion and lattice mismatch on the band gap.

Acknowledgments. This research is supported by ARO (W911NF1920041); NSF (DMR 1700137 and DMR 2218550); ONR (N0001416-1-2657 and N00014-20-1-2306);

the Center for Integrated Quantum Materials (NSF-DMR 1231319); and Brazilian the agencies CAPES (Gilvania Vilela/POS-DOC88881.120327/2016-01), FACEPE (APQ-05651.05/14), CNPq, and UPE (PFA/PROGRAD/UPE 04/2017). Work at Northeastern University was partially supported by the National Science Foundation (DMR-1905662) and the Air Force Office of Scientific Research Award (FA9550-20-1-0247). Work at São Paulo University was supported by FAPESP (2020/15570-0 and 2022/15791-2).

-
- [1] F. Natali, B. J. Ruck, N. O. V. Plank, H. J. Trodahl, S. Granville, C. Mayer, and W. R. L. Lambrecht, Rare-earth mononitrides, *Prog. Mater. Sci.* **58**, 1316 (2013).
- [2] C. M. Aerts, P. Strange, M. Horne, W. M. Temmerman, Z. Szotek, and A. Svane, Half-metallic to insulating behavior of rare-earth nitrides, *Phys. Rev. B* **69**, 045115 (2004).
- [3] I. N. Sivkov, O. O. Brovko, and V. S. Stepanyuk, Spin-polarized transport properties of GdN nanocontacts, *Phys. Rev. B* **89**, 195419 (2014).
- [4] A. Pal, K. Senapati, Z. H. Barber, and M. G. Blamire, Electric-field-dependent spin polarization in GdN spin filter tunnel junctions, *Adv. Mater.* **25**, 5581 (2013).
- [5] H. Yoshitomi, S. Kitayama, T. Kita, O. Wada, M. Fujisawa, H. Ohta, and T. Sakurai, Optical and magnetic properties in epitaxial GdN thin films, *Phys. Rev. B* **83**, 155202 (2011).
- [6] C.-G. Duan, R. F. Sabiryanov, J. Liu, and W. N. Mei, Strain induced half-metal to semiconductor transition in GdN, *Phys. Rev. Lett.* **94**, 237201 (2005).
- [7] S. Granville, B. J. Ruck, F. Budde, A. Koo, D. Pringle, F. Kuchler, A. Preston, D. Housden, N. Lund, A. Bittar, G. V. M. Williams, and H. J. Trodahl, Semiconducting ground state of GdN thin films, *Phys. Rev. B* **73**, 235335 (2006).
- [8] P. Wachter, Physical properties of stoichiometric GdN single crystals, *Results Phys.* **2**, 90 (2012).
- [9] T. S. Santos and J. S. Moodera, Spin filter tunneling, in *Spintronics Handbook: Spin Transport and Magnetism*, 2nd ed. (CRC Press, Boca Raton, 2019).
- [10] R. Vidyasagar, S. Kitayama, H. Yoshitomi, T. Kita, T. Sakurai, and H. Ohta, Study on spin-splitting phenomena in the band structure of GdN, *Appl. Phys. Lett.* **100**, 232410 (2012).
- [11] R. Vidyasagar, T. Kita, T. Sakurai, and H. Ohta, Giant optical splitting in the spin-states assisting a sharp magnetic switching in GdN thin films, *Appl. Phys. Lett.* **102**, 222408 (2013).
- [12] M. Azeem, Spin-split joint density of states in GdN, *Chin. Phys. Lett.* **33**, 027501 (2016).
- [13] D. Massarotti a, R. Caruso, A. Pal, G. Rotoli, L. Longobardi, G. P. Pepe, M. G. Blamire, and F. Tafuri, Low temperature properties of spin filter NbN/GdN/NbN Josephson junctions, *Phys. C (Amsterdam, Neth.)* **533**, 53 (2017).
- [14] H. G. Ahmad, M. Minutillo, R. Capecehatro, A. Pal, R. Caruso, G. Passarelli, M. G. Blamire, F. Tafuri, P. Lucignano, and D. Massarotti, Coexistence and tuning of spin-singlet and triplet transport in spin-filter Josephson junctions, *Commun. Phys.* **5**, 2 (2022).
- [15] R. J. Gambino, T. R. McGuire, H. A. Alperin, and S. J. Pickart, Magnetic properties and structure of GdN and GdN_{1-x}O_x, *J. Appl. Phys.* **41**, 933 (1970).
- [16] S. Cwik, S. M. J. Beer, S. Hoffmann, M. Krasnopolski, D. Rogalla, H.-W. Becker, D. Peeters, A. Ney, and A. Devi, Integrating AlN with GdN thin films in an in situ CVD process: Influence on the oxidation and crystallinity of GdN, *ACS Appl. Mater. Interfaces* **9**, 27036 (2017).
- [17] H. J. Trodahl, A. R. H. Preston, J. Zhong, and B. J. Ruck, Ferromagnetic redshift of the optical gap in GdN, *Phys. Rev. B* **76**, 085211 (2007).
- [18] R. Vidyasagar, T. Kita, T. Sakurai, and H. Ohta, Electronic transitions in GdN band structure, *J. Appl. Phys.* **115**, 203717 (2014).
- [19] F. Leuenberger, A. Parge, W. Felsch, K. Fauth, and M. Hessler, GdN thin films: Bulk and local electronic and magnetic properties, *Phys. Rev. B* **72**, 014427 (2005).
- [20] J. Tauc, Optical properties and electronic structure of amorphous Ge and Si, *Mater. Res. Bull.* **3**, 37 (1968).
- [21] A. R. Zanatta, Revisiting the optical bandgap of semiconductors and the proposal of a unified methodology to its determination, *Sci. Rep.* **9**, 11225 (2019).
- [22] A. Shaib, F. Natali, J. R. Chan, F. Ullstad, W. F. Holmes-Hewett, J. D. Miller, B. J. Ruck, and H. J. Trodahl, Coexisting structural phases in the catalytically driven growth of rock salt GdN, *Mater. Res. Express* **7**, 046404 (2020).
- [23] K. Senapati, T. Fix, M. E. Vickers, M. G. Blamire, and Z. H. Barber, Structural evolution and competing magnetic orders in polycrystalline GdN films, *Phys. Rev. B* **83**, 014403 (2011).
- [24] P. Wachter and E. Kaldis, Magnetic interaction in GdN and GdN_{1-x}O_x, *J. Magn. Magn. Mater.* **15-18**, 305 (1980).
- [25] K. Khazen, H. J. von Bardeleben, J. L. Cantin, A. Bittar, S. Granville, H. J. Trodahl, and B. J. Ruck, Ferromagnetic resonance study of GdN thin films with bulk and extended lattice constants, *Phys. Rev. B* **74**, 245330 (2006).
- [26] D. X. Li, Y. Haga, H. Shida, T. Suzuki, Y. S. Kwon, and G. Kido, Magnetic properties of stoichiometric Gd mononitrides, *J. Phys.: Condens. Matter* **9**, 10777 (1997).
- [27] F. Natali, S. Vézia, S. Granville, B. Damilano, H. J. Trodahl, E.-M. Anton, H. Warring, F. Semond, Y. Cordier, S. V. Chong, and B. J. Ruck, Molecular beam epitaxy of ferromagnetic epitaxial GdN thin films, *J. Cryst. Growth* **404**, 146 (2014).
- [28] J. R. Chan, S. Vézian, J. Trodahl, M. Al Khalifioui, B. Damilano, and F. Natali, Temperature-induced four-fold-on-six-fold symmetric heteroepitaxy, rocksalt SmN on hexagonal AlN, *Cryst. Growth Des.* **16**, 6454 (2016).
- [29] Y. P. Varshni, Temperature dependence of the energy gap in semiconductors, *Physica* **34**, 149 (1967).
- [30] P. B. Allen and M. Cardona, Temperature dependence of the direct gap of Si and Ge, *Phys. Rev. B* **27**, 4760 (1983).

- [31] S. Gaponenko and H. Demir, Quantum confinement effects in semiconductors, in *Applied Nanophotonics* (Cambridge University Press, Cambridge, 2018), pp. 52–91.
- [32] P. Dey, J. Paul, J. Bylsma, D. Karaiskaj, J. M. Luther, M. C. Beard, and A. H. Romero, Origin of the temperature dependence of the band gap of PbS and PbSe quantum dots, *Solid State Commun.* **165**, 49 (2013).
- [33] M. Li and J. C. Li, Size effects on the band-gap of semiconductor compounds, *Mater. Lett.* **60**, 2526 (2006).
- [34] M. Singha, B. M. Taelle, and M. Goyal, Modeling of size and shape dependent band gap, dielectric constant and phonon frequency of semiconductor nanosolids, *Chin. J. Phys.* **70**, 26 (2021).
- [35] A. Barnasas, N. Kanistras, A. Ntagkas, D. I. Anyfantis, A. Stamatelatos, V. Kapakli, N. Bouropoulos, E. Mystiridou, P. Pouloupoulos, C. S. Garoufalos, and S. Baskoutas, Quantum confinement effects of thin ZnO films by experiment and theory, *Phys. E* **120**, 114072 (2020).
- [36] B. Bertheville, H. Bill, and H. Hagemann, Experimental Raman scattering investigation of phonon anharmonicity effects in Li₂S, *J. Phys.: Condens. Matter* **10**, 2155 (1998).
- [37] D. A. Shohonov, D. B. Migas, A. B. Filono, V. E. Borisenko, R. Takabe, and T. Suemasu, Effects of lattice parameter manipulations on electronic and optical properties of BaSi₂, *Thin Solid Films* **686**, 137436 (2019).
- [38] G. Kim and S. Ahn, Thermal conductivity of gadolinium added uranium mononitride fuel pellets sintered by spark plasma sintering, *J. Nucl. Mater.* **546**, 152785 (2021).
- [39] W. M. Yim and R. J. Paff, Thermal expansion of AlN, sapphire, and silicon, *J. Appl. Phys.* **45**, 1456 (1974).
- [40] P. Y. Yu and M. Cardona, *Fundamentals of Semiconductors: Physics and Materials Properties*, 4th ed. (Springer, New York, 2010).
- [41] J. I. Pankove and D. A. Kiewit, Optical processes in semiconductors, *J. Electrochem. Soc.* **119**, 156Ca (1972).
- [42] X. Tang, F. Hossain, K. Wongchotigul, and M. G. Spencer, Near band-edge transition in aluminum nitride thin films grown by metal organic chemical vapor deposition, *Appl. Phys. Lett.* **72**, 1501 (1998).
- [43] J. A. Pérez Taborda, H. Riascos Landázuri, and L. P. V. Londoño, Correlation between optical, morphological, and compositional properties of aluminum nitride thin films by pulsed laser deposition, *IEEE Sens. J.* **16**, 359 (2016).
- [44] A. K. Harman, S. Ninomiya, and S. Adachi, Optical constants of sapphire (α -Al₂O₃) single crystals, *J. Appl. Phys.* **76**, 8032 (1994).